

View Article Online
View Journal

Journal of Materials Chemistry B

Materials for biology and medicine

Accepted Manuscript

This article can be cited before page numbers have been issued, to do this please use: K. Schickle, M. Goda-Cpa, Z. Parlak Vuslat, N. Grigorev, G. Desante, A. Chlanda, O. Mazuryk, K. Neuhaus, C. Schmidt, N. Amousa, K. Drozdz, S. Neuss, W. Pajerski, M. Esteves-Oliveira, M. Brzychczy-Woch, A. Kotarba and J. Gonzalez Julian, *J. Mater. Chem. B*, 2023, DOI: 10.1039/D3TB01854G.



This is an Accepted Manuscript, which has been through the Royal Society of Chemistry peer review process and has been accepted for publication.

Accepted Manuscripts are published online shortly after acceptance, before technical editing, formatting and proof reading. Using this free service, authors can make their results available to the community, in citable form, before we publish the edited article. We will replace this Accepted Manuscript with the edited and formatted Advance Article as soon as it is available.

You can find more information about Accepted Manuscripts in the <u>Information for Authors</u>.

Please note that technical editing may introduce minor changes to the text and/or graphics, which may alter content. The journal's standard <u>Terms & Conditions</u> and the <u>Ethical guidelines</u> still apply. In no event shall the Royal Society of Chemistry be held responsible for any errors or omissions in this Accepted Manuscript or any consequences arising from the use of any information it contains.



View Article Online DOI: 10.1039/D3TB01854G

ARTICLE

Revealing bactericidal events on graphene oxide nano films deposited on metal implant surfaces.

Received 00th January 20xx, Accepted 00th January 20xx

DOI: 10.1039/x0xx00000x

Published on 01 December 2023. Downloaded by WESTFALISCHE WILHELMS UNIVERSITAT MUNSTER on 12/5/2023 12:01:42 PM

Karolina Schickle^{a,b*}, Monika Gołda-Cępa^{c*}, Zümray Vuslat-Parlak^a, Nikita Grigorev^a, Gaelle Desante^a, Adrian Chlanda^d, Olga Mazuryk^c, Kerstin Neuhaus^e, Christina Schmidt^e, Nima Amousa^a, Kamil Drożdź^f, Sabine Neuss^{g,h}, Wojciech Pajerskiⁱ, Marcella Esteves-Oliveira^b, Monika Brzychczy-Włoch^f, Andrzej Kotarba^c, Jesus Gonzalez-Julian^a

At a time when pathogens are developing strong resistance to antibiotics, ,the demand for microbe-killing surfaces on implants has increased significantly. To achieve this goal, profound understanding of the underlying mechanisms is crucial. We show that graphene oxide (GO) nano-films deposited on stainless steel (SS316L) exhibit superior antibacterial features. The physicochemical properties of GO itself have a crucial impact on the biological events and their diversity may account for the contradictory results reported elsewhere. However, essential properties of GO coatings, such as oxygen content and resulting electrical conductivity, have been overlooked so far. We hypothesized that the surface potential and electrical resistance of the oxygen content in the GO-nano films may induce bacteria-killing events on the conductive metallic substrates. In our study, GO applied contains 52 wt.% of oxygen, thus exhibits insulating properties. Deposited as nano-film on an electrical conducting steel substrate, GO flakes induce a Schottky-barrier in the interface, which, in consequence, inhibits the transfer of electrons to the conducting, underlying substrate. Deposited as nano-film on an electrical conducting steel substrate, GO flakes can induce Schottky-barrier in the interface, which, in consequence, inhibits the transfer of electrons to the conducting, underlying substrate. Consequently, this generates reactive oxygen species (ROS), resulting in bacteria-death. We confirmed the presence of GO coatings and their hydrolytic stability by using X-ray photoelectron spectroscopy (XPS) XPS, μRaman spectroscopy, scanning electron microscopy (SEM), and Kelvin probe force microscope (KPFM) measurements. The biological evaluation was performed on the MG63 osteoblast-like cell line and two selected bacteria species: S. aureus and P. aeruginosa, demonstrating both, cytocompatibility and antibacterial behavior of GOcoated SS316L substrates. We propose a two-step bactericidal mechanism: electron transfer from the bacteria membrane to the substrate, followed by ROS generation. This mechanism is supported by changes in contact angle, surface potential, and work function, identified as decisive factors.

Introduction

Metallic surgical implants have become widespread materials over the past hundred years. Additionally to CoCr and Ti-based alloys, stainless steel is the widely used metal for various implants. Stainless steel finds applications in numerous branches of medicine such as cardiology (e.g. stent, artificial

valve), orthopedy (e.g. plate, screw or pin for bone fixation, artificial joints), dentistry (e.g. orthodontic wire, filling), craniofacial surgery (e.g. plate, screw), and otorhinolaryngology (e.g. artificial eardrum) ¹.

Although the research in implantology has made a huge effort, complications, and rejections still have severe consequences on a patient's health. Complications occur not only because of material failure, aseptic loosening, implant corrosion but also in case of allergic reactions or periprosthetic infections. Due to the poor surface performance at the interface of metal implants, the improvement of biocompatibility and chemical resistance in a physiological environment is required ². In the constant battle against harmful bacteria and infectious diseases, the development of antibacterial surfaces has emerged as a cuttingedge solution. These surfaces are designed to prevent the growth and proliferation of harmful microorganisms, enhancing hygiene and safety in various environments. Silver, known for its antimicrobial properties, has been harnessed through nanotechnology to create highly effective antibacterial surfaces. Silver nanoparticles release ions that can inhibit

a Institute of Mineral Engineering, RWTH Aachen University, Aachen, Germany b Department of Restorative Dentistry and Endodontology, Justus-Liebig-University Giessen, Germany

c Faculty of Chemistry, Jagiellonian University in Krakow, Poland

d Łukasiewicz Research Network - Institute of Microelectronics and Photonics, Flake Graphene Research Group, Warsaw, Poland

e Institute of Energy and Climate Research (IEK-12): Helmholtz-Institute Münster, Forschungszentrum Jülich GmbH, Münster, Germany

f Department of Molecular Medical Microbiology, Chair of Microbiology Faculty of Medicine, Jagiellonian University Medical College, Krakow, Poland g Helmholtz Institute for Biomedical Engineering, Biointerface Group, Universtiy Clinics

RWTH Aachen, Germany h Institute of Pathology, University Clinics RWTH Aachen, Germany i InnoRenew CoE, Livade 6a, 6310 Izola, Slovenia

^{*} These authors contributed equally to this publication and are corresponding authors: k.schickle@ghi.rwth-aachen.de and mm.golda@uj.edu.pl

bacterial growth by disrupting cell membranes and interfering with cellular processes. By incorporating these nanoparticles into various materials, the surfaces with long-lasting antibacterial properties can be created ³. On the other hand nature provides us with a wealth of inspiration for antibacterial solutions. Peptides, short chains of amino acids, have shown great promise as a non-toxic and sustainable means of combating bacteria. Some peptides can mimic the body's natural defence mechanisms or target specific bacterial strains. When integrated into surfaces, these peptides can prevent bacterial colonization and biofilm formation 4. Other strategy to achieve antibacterial features is an altering the physical and properties of surfaces through biomimetic nanostructuring 5, 6. Nanostructured surfaces can exhibit unique topographies and chemistries that can disrupt bacterial adherence and growth.

The application of graphene-based coatings, such as graphene oxide or reduced graphene oxide, can effectively modify both the chemical composition and the surface topography of metallic implants, leading to the induction of antibacterial mechanisms. There are several promising reports on GO-coated SS316L exhibiting lower toxicity than bare SS316L towards neuronal cells 7, and on GO-coated titania stimulating osteogenic activity of mesenchymal stem cells and improving biocompatibility to connective tissue cells 8. Moreover, as a oneatom-thick carbon lattice, graphene oxide is an excellent candidate to build a homogeneous and impermeable coating protecting metallic implants from oxidation and further damage induced by components of body fluids 9,10. Besides prevention of the corrosion events on the implant surfaces, GO-coatings could provide an additional advantage - antimicrobial and antibiofilm properties 11,12,9.

Published on 01 December 2023. Downloaded by WESTFALISCHE WILHELMS UNIVERSITAT MUNSTER on 12/5/2023 12:01:42 PM

The first indication that graphene derivatives could show an antibacterial behavior was presented on free graphene flakes 13. Here, the proposed and the most apparent bacteria-killing mechanism is based on the membrane stress and damage caused by the sharp edges of graphene nano-flakes. When attached to the surface, graphene shows also bacteria-killing features, but the proposed mechanisms differ. Two other bacteria-killing mechanisms are suggested for GO-nanofilms i) oxidative stress and ii) electron transfers 15. In the first suggested hypothesis, the reactive oxygen species (ROS) are generated by the GO-coating directly, provoking the deactivation of lipids and proteins and thus preventing further bacteria replication ¹⁶. Other scientists suspect antibacterial properties via electron transfer from negatively charged microbial membranes to positively charged graphene-coated substrates ¹⁷. The strong antimicrobial effect observed for GOcoated substrates appears to be indicated by changes in the surface potential of the evaluated biomaterials evoked by GO deposition. So far, several studies reported the impact of electrical properties of GO-coated substrates on the bacteria behavior ¹⁸. However, this phenomenon explaining the specific bacterial membrane/surface interactions has not been fully

understood nor quantified. The understanding Arofe othis mechanism is required to control interfacial reactions আৰু প্ৰাপ্ত কৰিছিল আৰু কিন্তু কৰিছিল। তাৰ minimize bacterial infection risks.

The adsorption of bacteria to the abiotic surfaces is mediated by electrostatic charges. The microorganisms suspended in liquids are charged and can be attracted or repelled by the biomaterial surface, depending on the dominating direction of the interaction potential. For biomaterials application it is critical to prepare surfaces that repel bacteria, therefore there are ongoing studies that try to resolve complex interface interactions between surfaces and biological moieties by the means of surface electronic properties (determined by work function) and bacterial cell surface charge (ζ -potential) ¹⁹. It was reported that understanding surface-bacteria electrostatic interactions can help to predict surface susceptibility to bacteria colonization, and thus risk of Biomaterials Centered Infections (BCI) ²⁰.

In the present study, we demonstrate a superior antibacterial behavior of GO-nano films deposited on SS316L substrates by modification of their electronic properties. Immobilization of GO-nano film on SS316L leads not only to the change in wettability but also the electrondonor properties. We suggest that the species with the most probable antibacterial mechanism involves two-steps - electron transfer from the bacterial membrane to the substrate and subsequent generation of the surface reactive oxygen species.

Results

The surface of the SS316L was first functionalized by silanization to obtain the -NH₂ termination on the SS316L substrates for enhancing the covalent attraction with the terminations of GO-flakes. The chemical composition of GO-flakes is summarized in Table 1. APDS molecules attach with the Self Assembled Monolayer (SAM) technique after hydrolyzation of its ethoxy groups. This hydrolysis creates Si-O- bonding with the –OH functional groups on the SS316L substrate. Free NH₂-groups are immobilized on the metallic substrate enabling further attachment to the epoxy groups of the GO flakes by ringopening or to the -OH groups (carboxyl or hydroxyl functions). Moreover, free amine groups can also act as corrosion retardants for metallic substrates due to their hydrophobic character ^{24,25}.

Table 1. Chemical composition of synthesized GO-flakes determined by combustion elemental analysis.

Element	Amount [%]
Oxygen	52.2
Carbon	42.3
Hydrogen	2.3
Sulphur	<1
Nitrogen	<0.4

Journal Name ARTICLE

Each step of the coating method was precisely verified with the use of XPS (Fig. 1) and µRaman (Fig. 2). Comparatively to our previous study on zirconia substrates, XPS spectra survey showed a similar evolution of the Si 2p, C 1s, and O 1s. In Fig. 1, wide scans (left panel) as well as Si 2p narrow scans (right panel) are presented proving the effectiveness of each coating step. In the wide scan spectra, the C 1s signal is more pronounced at each consecutive coating step, i.e. the lowest carbon content was observed for the SS316L parent samples (carbon content for SS316L alloy is 0.03%), the increase in C 1s is observed for SS316L silanized and SS316L+GO samples. The reason for that is the chemical composition of APDS, used for the silanization, consisting of Si, N and C elements, while graphene oxide coating consists exclusively of C and O. Moreover, the progressive disappearance of the Fe 2p and Cr 2p peaks for the silanized and GO-coated samples when compared to the SS316L shows the effectiveness of the coating process. Narrow scans for Si 2p further confirm the efficiency of the silanization process (SS316L silanized) and subsequent GO-coating (SS316L+GO). For the investigated samples the Si 2p peak becomes more intense after covering the surface with APDS and again less pronounced after GO deposition the Si 2p signal is attenuated as GO flakes cover the silane molecules. This was confirmed by quantifying the elements through XPS analysis, which indicated an increase in carbon content after GO-coating, while a decrease in Si 2p was observed (Supplementary document, Table S1).

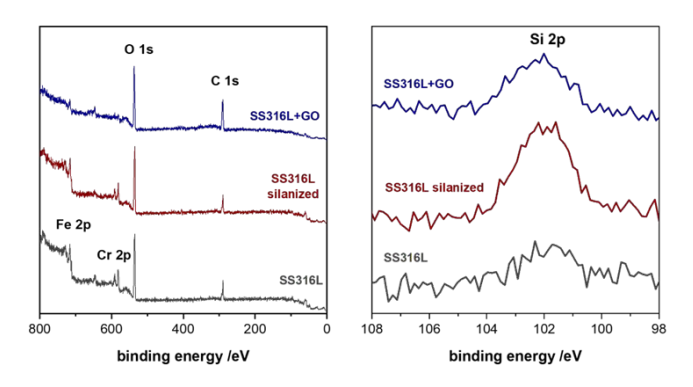


Fig. 1. XPS spectra of SS316L (reference samples), SS316L silanized (silanized samples), and SS316L+GO (GO-coated samples). The left panel presents a wide scan, where the C 1s and O 1s peaks become more intense after each step, proving the presence of the silane molecule on the surface (SS316L silanized), and subsequently the covering of the surface by GO (SS316L+GO). Fe 2p and Cr 2p signals present in the SS316L alloy become less intense, proving the effectiveness and integrity of the coating. The right panel summarizes narrow scans for Si 2p, confirming the effectiveness of the silanization process (SS316L silanized) and subsequent GO-coating (SS316L+GO).

In Fig. 2, representative μ Raman spectra of the investigated samples are presented and they are in accordance with the results obtained by XPS. The results obtained for the SS316L+GO confirm the presence of GO on the substrates since the spectra of the GO-coated samples exhibit a very similar profile as the graph of GO itself. The characteristic G and D peaks for the graphene-based materials were neither visible on

bare SS316L nor on silanized samples (SS316L silanized). Having in mind the potential application of the obtained materials and their further characterization e.g. with the use of biological tests, the stability of the coating was evaluated in the sonication bath. After exposure to ultrasounds, the samples were again examined with the use of RS, proving the stability of the coating over SS316L (Fig. 2 right).

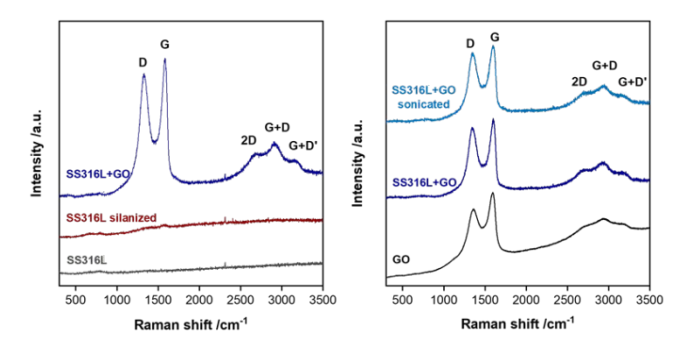


Fig. 2. Left: The representative μ Raman spectra confirming the GO coating on SS316L substrates. The spectrum obtained for the SS316L+GO samples shows characteristic maxima as for the GO reference samples (GO). Right: The representative μ Raman spectra confirm the stability of the GO coating over SS316L substrates after exposure to ultrasounds. The spectra obtained for the SS316L+GO sonicated and SS316L+GO samples show characteristic maxima for the GO reference samples (GO).

The obtained GO-coated samples were further investigated in terms of the coating integrity and surface topography. The GO coating on SS316L exhibited a wrinkled topography, as illustrated in SEM images presented in Fig. 3. The results obtained for the SS316L+GO are in line with other scientific reports ²⁶ and our previous experiments made on zirconia substrates ²¹. The flakes are well stretched out on SS316L substrates, proving that flakes have attached to the surface homogeneously. Moreover, the images taken for the SS316L+GO sonicated for 15 min confirmed again (Fig. 3 right panel) the stability of the coating after exposure to the ultrasounds.

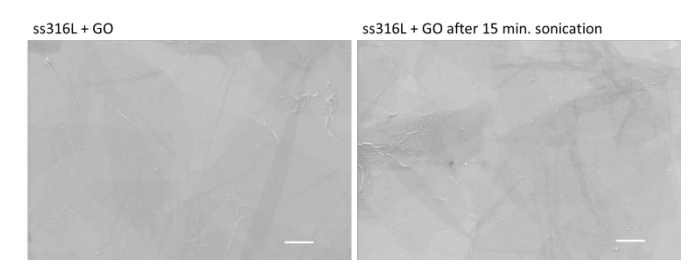


Fig. 3. SEM images of the SS316L+GO (left) and sonicated SS316L+GO (right) samples presenting the homogenous distribution of GO flakes over the SS316L surface and stability of the coating after exposure to ultrasounds. When overlapped, the GO flakes show a darker contrast (scale bars correspond to 0,5 μ m).

Surface properties determine the eucaryotic cells and bacteria responses to a biomaterial, therefore, wettability and electrondonor properties might be decisive in the biocompatibility with the targeted tissue and bacteria attachment to the biomaterial surface where the so-called race for the surface takes place ^{20,27}. Moreover, one of the theories

explaining the bactericidal effect of GO-coatings assumes that the transfer of electrons from the microbial membrane to the GO surface stimulates antibacterial activity 28 . Therefore, the wettability of the obtained samples as well as their surface work function were measured. As presented in Fig. 4, the bare SS316L samples are hydrophobic with a water contact angle (θ w) = 92°, and the GO-coated samples become hydrophilic with a significant drop of θ w down to 73°.

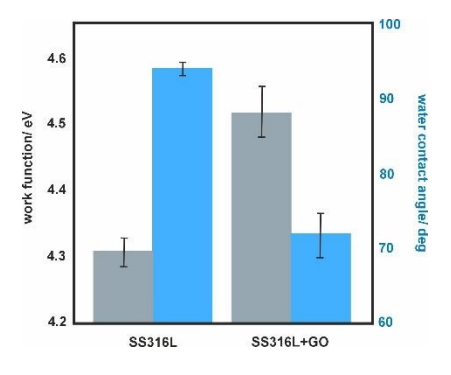


Fig. 4. The results of water contact angle and work function measurements for the bare SS316L and SS316L+GO.

Published on 01 December 2023. Downloaded by WESTFALISCHE WILHELMS UNIVERSITAT MUNSTER on 12/5/2023 12:01:42 PM

Moreover, there is also a significant difference in measured work function values between bare SS316L Φ = 4.3 eV and coated SS316L+GO Φ = 4.5 eV samples. In addition, it is also worth saying that the charge transfer of graphene-based materials can also be driven by the number of carbon layers. In general, charge—transfer tends to be more efficient for thinner graphenic layers $^{29}.$

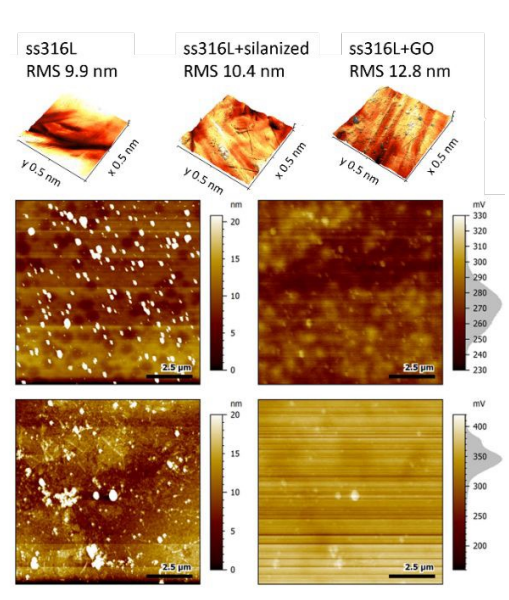


Fig. 5. (top) 3D AFM topographical maps of tested samples: (left) bare 316L surface, (middle) silanized 316L surface, (right) silanized 316L surface coated with GO flakes; and exemplary images of the pure SS316L (middle) and SS316L-GO (bottom): on the left hand are the topography images and on the right hand are corresponding KPFM images. To show the range of the surface potential, a histogram of the measured surface potential values is indicated at the palette of the KPFM images. Stripes in the KPFM image of SS316L-GO are artefacts which can be attributed to poor electronic surface conductivity of the sample.

Subsequent control measurements of the surface potential with KPFM under Ar atmosphere were performed / Where 8the samples were previously dried under Ar flux. KPFM is performed in intermittent contact mode with the AFM cantilever vibrating at its resonance frequency. Additionally, an AC potential is applied to the AFM tip which is varied by interaction with the sample. An additional DC voltage, which is directly equivalent to the surface potential, is applied to compensate the contact potential difference between the sample and the probe constantly restoring the original phase and amplitude of the AC signal. The surface potential measured by KPFM is directly equivalent to the Volta potential under specific conditions (smooth and clean sample, no adsorbed species), which means that it is extremely sensitive even for small changes of the local Fermi level. Humidity from air or other species adsorbed on the sample surface will act as screening charges which can strongly influence the measurement.

In this case, the measured dry samples showed a mean surface potential of 273±16 mV for bare SS316L and 347±43 mV for coated SS316L+GO (Fig. 5). The surface potentials were measured at an average tip-sample distance of 30 nm and mean surface potentials were averaged over seven images at different sample locations. Calculation of the work function from the surface potential led to values of Φ = 4.29±0.02 eV for SS316L and Φ = 4.21±0.04 eV for SS316L+GO, which are in good accordance with the macroscopic work function values determined based on Kelvin measurements. Since GO is also used as a humidity sensor, a dependence of the surface potential/work function on the sample humidity is a prerequisite. It can be assumed that the work function will strongly depend on direct contact with liquids, even though this is not directly measurable.

The surface of the GO-coated samples was further evaluated with the use of AFM, to visualize the topography and calculate surface roughness (RRMS). The results are summarized in Fig. 5, where AFM images of bare SS316L, SS316L silanized and SS316L+GO are presented together with corresponding roughness. The bare surface of SS316L is rather smooth with minor corrugations and RRMS = 9.9 nm, after the silanization process some irregularities are visible together with the slight increase in RRMS to 10.4 nm. The most pronounced changes are visible for GO-coated samples (SS316L + GO), where wrinkled GO flakes are detected, similar to the one observed with SEM (Fig. 3), for the SS316L + GO samples. Additionally, a significant increase in RRMS up to 12.8 nm is observed. In order to measure the thickness of the coating, the adhered layer was intentionally scratched with a wooden stylus. The thickness of GO-coating was measured by AFM: 61.3 ± 7.4 nm. This value was additionally confirmed by independent focus ion beam and scanning transmission electron microscope (FIB and STEM, respectively, Helios 5 Hydra DualBeam, ThermoFisher Scientific, MA, USA) measurements, were the thickness of the coating

Journal Name ARTICLE

varied between 60-70 nm (supplementary document, figure S2).

The cytocompatibility of GO-nano films on SS316L substrates was evaluated by using live/dead staining following ISO 10993-5. MG63 osteoblast-like cells were used in this study as a relevant model for future applications of the obtained approaches. i.e. bone replacement materials. representative images of live/dead-stained cells on glass (control), SS316L and SS316L coated with GO-nano films are presented in Fig. 6. The cells attached intensely to all tested surfaces, showing a typical, well-spreaded morphology, demonstrating a high rate of viability within incubation times. Moreover, the cells were counted after one, three and seven days of incubation to quantify the proliferation rate. In the diagram presented in Fig. 7, it can be observed that the most rapid proliferation was observed between the 3rd and 7th day of incubation on each tested sample. Interestingly, the lowest number of viable cells after the 7th day was detected on bare SS316L samples, showing also a higher amount of dead cells (under 5%). This could indicate that the GO-nano film creates an anti-corrosive barrier, reducing the release of toxic metallic ions from the SS316L substrate surface.

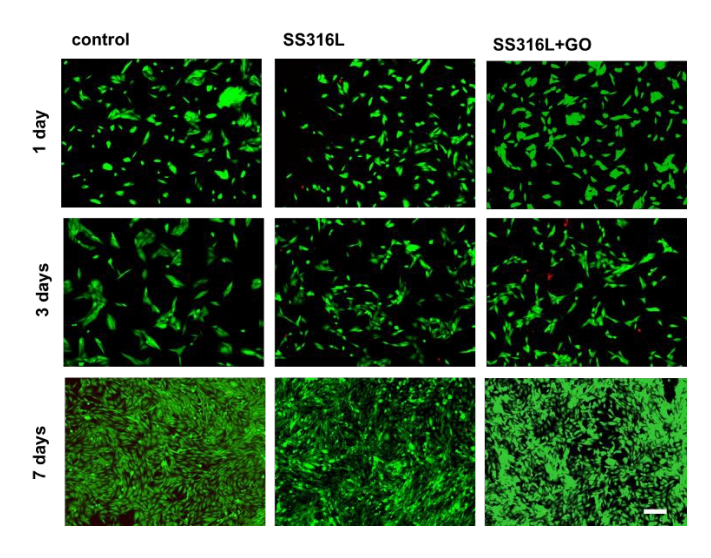


Fig. 6. Proliferation and viability fluorescence images of live/dead stained MG63 cells seeded on glass (control), SS316L and SS316L coated with GO-nano film (SS316L+GO) after 1. 3 and 7 days of incubation. Scale bars correspond to 200 um.

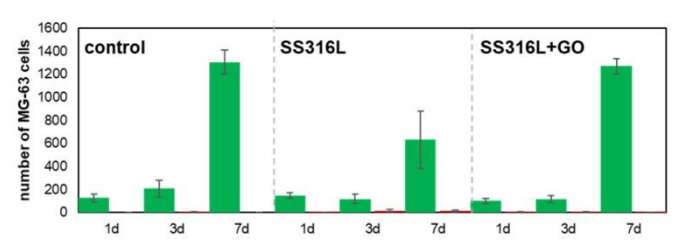


Fig. 7 The number of viable (green bars) and dead (red bars) MG63 cells on the control, SS316L and 316L+GO samples after 1, 3 and 7 days of incubation presenting the proliferation rate of the cells.

Biological evaluation of the biomaterials should also take into consideration the risk of infection, as approx. 2% 67% he patients that undergo implantations require revision surgery due to implant-related infections 30. Consequently, in our study, we used two bacteria strains that most commonly cause postsurgery complications, i.e. Gram-negative P. aeruginosa and Gram-positive S. aureus. In Fig. 8 the representative results of live/dead staining are presented. The fluorescence images of dead (red) and viable (green) bacteria on the investigated samples: glass (control), SS316L and SS316L+GO after 1 and 4 hours of incubation. It can be seen that the bacteria adhere to the investigated surfaces in a different manner. P. aeruginosa after 1 hour of incubation homogeneously covered the surfaces of SS316L and SS316L+GO, without large bacteria agglomerates. After 4 hours of incubation, a significant change can be seen for the surface of SS316L+GO, where the majority of the cells are stained dead and form clusters. After 4 hours of incubation, for S. aureus also major changes were observed between bare SS316L and GO-coated SS316L samples. The surface of uncoated samples is covered with viable S. aureus cells which already started to agglomerate and form 3D structures which indicates early biofilm formation. In contrast, at the surface of SS316L+GO, the majority of the bacterial cells are dead (red bright spots).

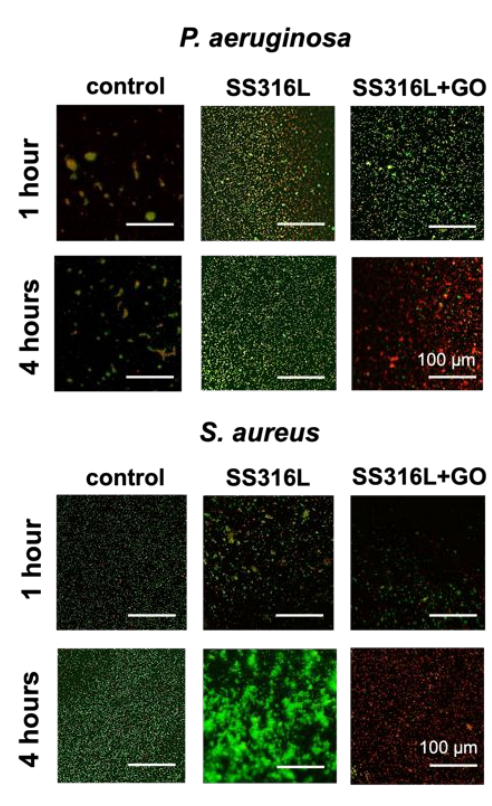


Fig. 8. Representative fluorescence images of live/dead stained bacteria (merged channels): P. aeruginosa and S. aureus after one and four hours of incubation on control (glass), SS316L and SS316L+GO samples. Red-stained cells correspond to dead and green to viable cells respectively.

The area occupied by bacteria was calculated based on fluorescence microscopy images (representatives are

presented in Fig. 8). In the plots presented in Fig. 9 it can be seen that the total area occupied by bacteria, which is the sum of red and green bars, differs significantly for P. aeruginosa and S. aureus. After 1 h of incubation, the largest total area occupied by Gram-negative P. aeruginosa was observed for the bare SS316L (4.5% of the available area), while at GO-coated samples it was slightly lower (2.4%) but somehow higher than the one for the control (1.7%). The trend is similar for a longer time of incubation, however, the differences are more pronounced. The total area occupied by bacteria is also the highest for the bare SS316L (7.3%), lowest for control (2.7%) and moderate for GO-coated samples (4%). Moreover, as can be seen in Fig. 9, after 4 hours of incubation on the SS316L+GO, all of the bacteria present at the surface are dead (red bar) which indicates the antimicrobial activity of the GO coating over the SS316L substrate. For the Gram-positive S. aureus, the total area occupied by bacteria after 1h of incubation is largest for the control samples (3.5%) and comparable for bare SS316L and SS316L+GO (2.1% and 1.8%, respectively). For S. aureus the dramatic difference can be observed after 4h of incubation, i.e. there is a significant increase in the number of bacteria at the surface for the control sample (14%), while for bare SS316L and SS316L+GO, the total area occupied by bacteria is quite similar (4.9% and 6%, respectively). Also, after 4 hours of incubation, the antibacterial activity against S. aureus of the GO-coated samples can be observed, as the majority (5.3%) of the bacteria were dead.

In summary, for both bacterial strains, the strong antibacterial effect of GO coating is observed after 4h of incubation when the majority of the bacterial cells are dead.

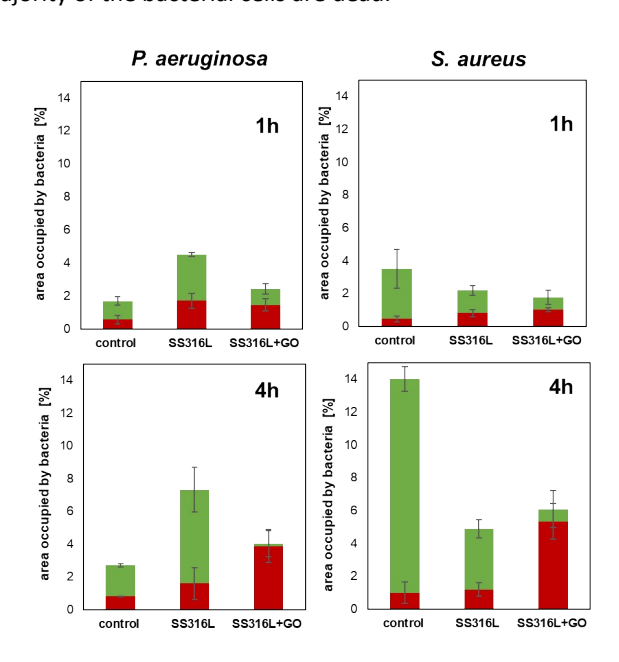


Fig. 9. Total area occupied by P. aeruginosa and S. aureus bacteria strains after 1 h and 4 h of incubation with the glass (control), SS316L and SS316L+GO samples.

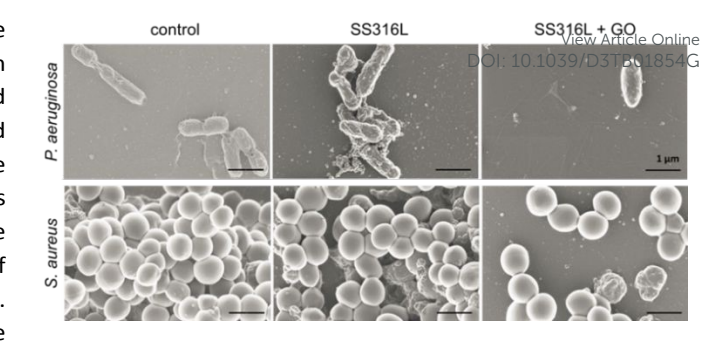


Fig. 10. SEM images of P. aeruginosa and S. aureus seeded on glass (control), SS316L and SS316L+GO after 24 h of incubation. Scale bars correspond to $1~\mu m$.

To determine the differences in the biofilm formation at the investigated surfaces, after 24h of incubation with P. aeruginosa and S. aureus, SEM analyses was performed. As can be seen in Fig. 10, P. aeruginosa on control and bare SS316L formed some clusters of few cells, while on the SS316L+GO, only a few single, non-agglomerated bacteria were found. After the same incubation time, S. aureus was able to form thick layers of cells over the bare SS316L, while on the SS316L+GO the formation of biofilm was slower as significantly fewer agglomerated bacteria were observed. The obtained results proved that the GO coating over SS316L is antibacterial against both gram-negative P. aeruginosa and Gram-positive S. aureus and effectively limits the biofilm formation of Gram-negative P. aeruginosa.

The evaluation of ROS formation by the uncoated and GO-coated surfaces, both after one and four hours of incubation, is presented in Figure 11. To evaluate the statistically significant differences we ran one-way ANOVA with post-hoc Tukey HSD Test, statistically significant values are marked in Fig.11, significant differences were *p<0.01 unless otherwise specified. This indicates that both groups exhibited comparable and continuously increasing values of ROS production. The measured ROS values can be attributed to $\rm H_2O_2$ produced by redox reactions on the sample surfaces upon contact with the aqueous medium.

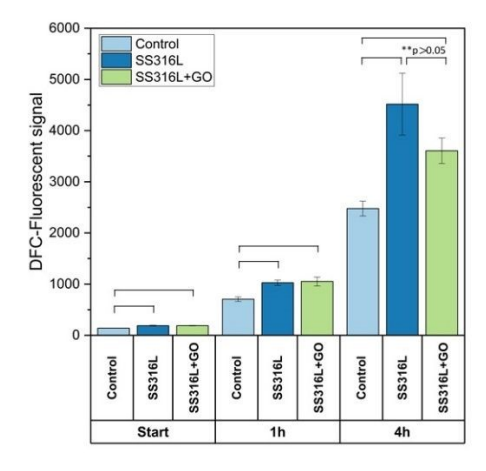


Fig. 11. ROS formation of SS316L and SS316L+GO after incubation in PBS for one and four hours, corresponding to the incubation intervals during bacterial tests compared with the control PBS.

Published on 01 December 2023. Downloaded by WESTFALISCHE WILHELMS UNIVERSITAT MUNSTER on 12/5/2023 12:01:42 PM

Journal Name ARTICLE

Discussion

Bactericidal properties of implant surfaces are in great demand, especially in the medical field. The ultimate aim is to develop smart surfaces that exhibit antibacterial properties without compromising their cytocompatible and even bioactive features. Flake graphene and its derivatives have been proposed as suitable coating materials for implants since they exhibit both, cytocompatibility and antibacterial properties ³¹. In our previous study, we presented an innovative method for the functionalization of inert ceramic surfaces by covalent immobilization of GO-nano films ²¹. Here, we demonstrate that this method could successfully be adopted for metal substrates, such as medical-grade stainless steel (SS316L).

An intact, homogeneously distributed as well as hydrolytically stable coating was obtained (Fig. 1-5). The hydrolytic stability of biomaterials is of great importance as they are exposed to a harsh and corrosive environment of body fluids. GO-nano films deposited on SS316L were found to be a suitable surface for cell attachment and proliferation due to the chemical properties and the observed cell behavior (Fig. 6-7). The proliferation was observed within the incubation time from 1 to 7 days, showing the low numbers of dead MG63-cells (significantly below 5%), which is the first indication for cytocompatibility according to ISO10993-5. Neither a negative influence in the manner of viability, apoptosis and necrosis nor morphological changes of the cultured cells on the GO nano-film compared to bare SS316L as well as the glass control could be observed. At the same time, as revealed by conducted microbiological tests, the GO-coated samples proved to be antibacterial against P. aeruginosa and S. aureus (Fig. 8-10). By effectively decreasing the number of bacteria attaching to the surface as well as delaying the onset of biofilm formation. As a result, the coating can limit the risk of post-surgery infection and favour osteoblasts in the "race for the surface" of implantable materials.

The antibacterial behavior of graphene-based materials has not yet been explained and fully understood, and the literature reports are inconclusive, presenting contrary results 9,32,33. One of the theories states, that GO, while contacting with the liquid medium initiates spontaneous ROS formation, provoking the deactivation of lipids and proteins and thus preventing bacteria proliferation 12. Here, the antibacterial behavior of GO-coated conductive substrates is linked to the direct production of ROS by the material itself. Since there were no significant differences in ROS values between GO-coated and uncoated SS316L, it suggests that the bacteria-killing cascade is likely triggered by the direct contact of bacteria with the substrate. Owing to the obtained results regarding determination of ROS generated in the PBS by the GO-surface itself, we can exclude an antibacterial mechanism based on this hypothesis. By these results we could prove, that in case of our coatings, the ROS formation was comparable or even slightly higher by SS316L uncoated than GO-coated substrates after one as well as four hours of

incubation. Since no significant difference was observed, other processes must be involved in the bacteria killing events of Go. coated SS316L specimens (Fig. 11). Therefore, our results indicate that the mechanism of indirect ROS formation, involving electron transfer that subsequently leads to ROS production, may be a more probable mechanism. This hypothesis aligns with suggestions made in the cited literature. ³⁴. Even though the evidence of the electron-transfer involvement in the bactericidal surface events is apparent, the clarification of the processes in the nanoscale on these surfaces is still insufficient. Our results strongly support the theory of electron transfer that triggers the bactericidal effect and explains some of the processes taking place at the implant-cell interface. Therefore, we hypothesize that the large-area GOnano films deposited on SS316L by applying the dip coating method create the electrostatic environment leading to bacterial death 35. When graphene oxide (GO) is deposited on substrates exhibiting high electrical conductivity, it gives rise to a minute energy barrier known as a Schottky nano-barrier. This barrier emerges from the variance in fundamental energy levels between the GO coating material and the substrate, typically defined by the Fermi level. Consequently, this energy barrier has a notable impact on the flow of electrical current at the junction (Fig. 12). Following this hypothesis, by direct contact and adsorption of the bacteria to the GO-coated SS316L, the electrons released from the negatively charged bacterial membrane (-11 mV for P. aeruginosa, -12 mV for S. aureus) [20] are attracted by SS316L substrate surface. The hypothesis that electrons are transferred from bacterial cell walls toward the interface can be supported by the experimental data obtained in this study. For the surfaces with higher work function values electron transfer to oxygen molecules is less likely, therefore the electron transfer from the bacteria seems to be favorable. Such electron transfer energetically subsequently result in the formation of negatively charged reactive oxygen species in the vicinity of the bacteria cell walls, and thus damage them. Moreover, since the zeta potentials of the investigated bacteria do not differ, it can be concluded that during the attachment of bacterial cells, the electronic properties of the surface play the primary role, which was also observed in our previous studies 19,20,36.

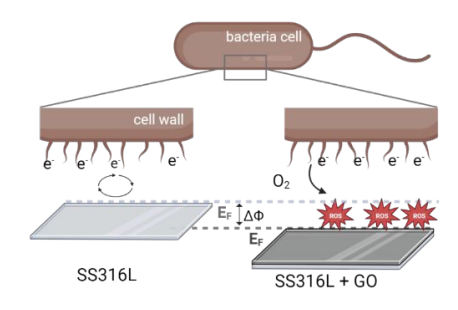


Fig. 12. Scheme of electronic interactions at the bacteria-surface interface for bare SS316L and coated with GO-nanofilm showing the effect of coating on the electron transfer processes. ROS formation at the interface is proposed to involve -OH and -COOH functional groups, initially present in the GO-nanofilm.

View Article Online DOI: 10.1039/D3TB01854G

ARTICLE Journal Name

The conductivity of the coating is strongly influenced by the fine tailoring of the oxidation level of graphene oxide ³⁷. The applied GO nanoflakes exhibit 52 wt. % of the oxygen content. According to the literature, graphene itself is defect-free and thus a highly conductive material (106 S cm⁻¹), while with the oxygen content, due to the high quantity of carboxyl and carbonyl groups in the structure, the material becomes isolating (<0.001 S cm⁻¹) ³⁸. It can therefore be stated that the higher the oxygen content on the surface of GO flakes, the lower the electrical conductivity. According to the values reported in the literature, the electrical conductivity of GO containing over 50 wt. % oxygen does not exceed 0.001 S cm⁻¹, which corresponds to a very low electrical conductivity behavior 37. This is in accordance with our results of work function values before and after GO deposition on the SS316L surface (Fig. 4). The values of the work function increase from 4.3 to 4.5 eV after deposition of GO-nano film, since the work function values depend on both, chemical potential and the surface dipole, generating an additional barrier to remove the electron from the surface. The increment of a work function together with the positive surface potentials measured for both SS316L and the GO coating, also supports our conclusion that the electron transfer direction occurs from bacteria to the material surface. So far, minor attention has been focused on this aspect, specifically regarding oxygen content, which strongly affects GO properties. This could be a reason for inconsistencies in literature reports about antibacterial/bacteria-promoting features of GO and rGO 32. It is well established that graphene oxide is an electric insulator, but its conductivity can be tuned (raised) by restoration of honeycomb atomic structure, elimination of structural defects and oxygen-based functional groups, ergo through a reduction process. At this point, we want to underline that the removal of oxygen functional groups from GO flakes` surface depends upon reduction type (chemical, thermal, light, pressure, etc.) and conditions, which determine the electrical conductivity of resulting rGO flakes and strongly affects the biological responses 33. The surface terminations of GO play, especially by its electrical properties, a crucial role and can strongly influence the surface potential, already by slight modifications. By controlling the terminations of applied GO in combination with the electrical conductivity of the underlying substrates (attracting the electrons from the bacteria membrane), the bacteria-killing mechanisms could be controlled. Moreover, the work function and surface potential could be adjusted not only by the oxidation stage of GO but also by the coating thickness ^{37,39}. Our developed GO-coatings exhibit a thickness of 1-4 layers, whereas the single nano flakes structure shows a partially overlapping arrangement (Fig. 3 and 4). It is worth noticing, that besides coating itself, the substrate characteristic could also strongly influence the values of work function, in particular in the case of thin films due to the polarization effects at the interfacial area.

Published on 01 December 2023. Downloaded by WESTFALISCHE WILHELMS UNIVERSITAT MUNSTER on 12/5/2023 12:01:42 PM

Experimental

Substrate preparation. The stainless-steel substrates of 5x5x2 mm were coated with GO as shown in the supplementary document in figure S1, according to our protocol described elsewhere 17 .

GO was synthesized by the improved Hummers method called the modified Marcano method. Briefly, a mixture of H₂SO₄/H₃PO₄ (9:1) was added to graphite flakes. Then KMnO4 was added progressively in excess (6:1) to graphite. The oxidation reaction took place at 50°C and was stopped by the addition of ddH₂O, then H₂O₂. The sedimented slurry was then micro-filtered and ultimately washed and exfoliated. The obtained GO solution contained 2.5 g/L of GO. The chemical composition in terms of detection of oxygen amount of synthesized GO flakes was done with the combustion analyzer OH836 (Oxygen/Nitrogen/Hydrogen elemental analyzer, Leco, USA). The examination was performed in a helium atmosphere. Prior to the examination, the analyzer was calibrated according to the procedure described elsewhere ¹⁸. In brief, two calibration samples of known chemical composition were tested in order to verify the detection sensitivity of the experimental apparatus.

Subsequently, SS316L samples were heat-treated at 100°C for 1 h and coated with GO flakes using the dip-coating technique. For this purpose, the samples were dipped into the graphene oxide solution of 2.5 g/L. After 1 min of immersion, the samples were rinsed with ddH₂O and dried overnight at 40 °C.

The SS316L surfaces were modified by APDS silane. Briefly, the SS316L samples were placed in a solution of APDS-Toluene (1.5% APDS) at 120°C for two hours. Before silanization, the samples underwent 3 cleaning steps, in acetone, ethanol and ddH2O, successively. After silanization, the samples were rinsed three times with toluene and subsequently with ddH2O and underwent one-hour post-silanization treatment at 100°C. Such synthesized GO nanoflakes were subsequently deposited as GO-nano film by applying a dip-coating technique. To obtain an intact and well-distributed GO-nano film, SS316L substrates were immersed in 10 ml of 2.5 g/L GO solution for one minute and subsequently taken out by applying an adjusted withdrawal speed of 1mm/min. The samples were subsequently gently rinsed with ddH2O before drying.

Characterization. For verification of surface modification of the SS316L samples with graphene flakes (GO), X-ray photoelectron spectroscopy (XPS) measurements were performed. The evaluation was conducted in a UHV chamber with a vacuum level above 5 \times 10–9 mbar using a SESR4000 analyzer (Gammadata Scienta). The measurements were performed using the monochromatized Al-K α source (1486.6 eV) operated at 250 W with a pass energy of 100 eV for the survey and narrow scans. The obtained XPS spectra were calibrated for the C1s peak at 284 eV and analyzed using the commercially available software Casa-XPS 2.3.15.

Journal Name ARTICLE

 μ Raman spectroscopy was applied to access the structural changes of the investigated samples. The μ Raman spectra were obtained with the use of the Renishaw InVia spectrometer at an excitation wavelength of 514.5 nm. The spectra were recorded at room temperature with a 50× magnification lens in the characteristic range of 1000–3500 cm–1 for carbon materials. To maximize the signal-to-noise ratio, at least nine scans for each measurement were accumulated.

Scanning electron microscopy (SEM, GeminiSEM 500, Zeiss, Jena) showed the obtained intact coating, whose composition was subsequently determined by XPS and Raman spectroscopy. In addition, Kelvin Probe Force Microscopy (KPFM) measurements under Ar atmosphere using ASYELEC.01-R2 probes with Ti/Ir coating were performed to estimate the surface potential of the sample and support macroscopic measurements of the work function. Similar to the conventional Kelvin method described below, the work function of a sample can be calculated from the obtained surface potential measurements, when the work function of the AFM tip is previously determined by referencing to a material with a known work function (in this case titanium metal).

To determine the values of the work function (Φ) of the investigated samples, the contact potential difference (VCPD) measurements were performed by applying the Kelvin method with a KP6500 probe (McAllister Technical Services). The stainless-steel plate (diameter = 3 mm) was used as a reference electrode (Φ ref ≈ 4.3 eV) and the following settings were applied: the vibration frequency = 114 Hz, amplitude = 40 a.u, and the gradient of the peak-to-peak versus backing potential = 0.1. The final work function value of each sample was an average of at least 60 independent measurements performed at ambient conditions. The final values were calculated based on the relation: Φ sample = Φ ref – eVCPD.

The water contact angle measurements were carried out with the use of a goniometer (Surftens Universal Instrument, OEG GmbH, Frankfurt (Oder), Germany) to determine the wettability of investigated samples. Static contact angles were measured and calculated using windows image processing software (Surftens 4.3). For each sample, the mean value was obtained for five 2.0 µl water drops in three independent series.

The adhesion and stability of the coating on the metallic surfaces were proven through sonication (Elmasonic S 180H, Elma, Germany). The sonication was applied for 15 min on the samples immersed in 10 ml of ddH_2O . After sonication, samples were analyzed by SEM to visualize the GO-coating after the aggressive aging process.

Biological evaluation of the GO-coatings. Cytocompatibility evaluation was performed on uncoated and GO-coated SS316L-substrates in accordance to the International Organization for Standardization ISO10993-5. Briefly, live/dead stainings of the MG63 cell line (osteoblast-like cells, CRL-1427™, ATCC®, Manassas, VA, USA) on the specimens were evaluated after 1, 3, and 7 days of incubation. For this, 600 μl of Ringer solution (B. Braun, Melsungen, Germany) were mixed with 10 μL

fluorescein diacetate (FDA, 5 mg/mL in acetone, Sigma Aldrich, Steinheim, Germany) and 10 µL propidium in in in PBS, Sigma Aldrich, Steinheim, DE) and applied on the seeded cells. After 20 seconds of incubation, stained cells were analyzed by fluorescence microscopy (Zeiss Observer Z1, Zeiss, Jena, Germany). Green fluorescence indicates viable cells while red fluorescence labeled-dead cells.

The following reference microorganisms were used in the study: Staphylococcus aureus DSM 24167 (Deutsche Sammlung von Mikroorganismen und Zellkulturen), and Pseudomonas aeruginosa ATCC® 27853. The bacterial strains were incubated at 37°C in Bacto™ Tryptic Soy Broth (TSB, Becton Dickinson). After 24 h, bacterial cells were harvested by centrifugation (13000 rpm, 5 min) and washed 3 times with Dulbecco's Phosphate Buffered Saline (DPBS, Lonza). The bacterial pellets were resuspended in DPBS to obtain bacterial suspensions of ~3·108 CFU/mL (colony forming units) corresponding to 0.5 McFarland standard. The prepared bacterial suspensions were used in microbiological tests.

The ability of investigated samples for bacterial adhesion was investigated using a fluorescent microscope (BX63 Olympus) according to the previously described procedure ²⁰. The samples were incubated for 1 h and 4 h with prepared bacterial suspensions (0.5 McFarland, 1 ml suspension per well) at 37°C in the sterile 24-well plates. For each sample (bare SS316L and coated with GO), the tests were performed in triplicates for each bacterial strain. After the incubation, the samples were gently washed with DPBS to remove all non-attached bacteria and stained with the LIVE/DEAD™ BacLight™ Bacterial Viability Kit (Invitrogen™). For each sample at least 15 randomized images were taken, LIVE/DEAD channels were merged, and the area covered by the bacteria was measured using Java opensource ImageJ software 1.51 k ²³.

DCF fluorescence measurement was performed to evaluate the formation of reactive oxygen species (in particular H_2O_2) on SS316L and SS316L+GO. First, the DCF stock solution was prepared by mixing 2',7'-dichlorodihydrofluorescein diacetate (H2DCF-DA) with anhydrous ethanol, 0.01M NaOH and 0.1M TRIS-HCI. Samples were then placed in the 48-well plate and covered with the previously prepared dye solution. Three wells containing only the solution were measured as controls. The release of the reactive oxygen species oxidized H2DCF- and produced a fluorescence signal. The fluorescence signal was recorded in situ after one-, and four-hours immersion using the PerkinElmer LS55 spectrofluorimeter using the following excitation/emission wavelengths: 485/535 nm.

Conclusions.

GO-nano films have been successfully immobilized on SS316L substrates. The resulting GO-coated samples were found to be cytocompatible according to ISO 10993-5 and exhibit antibacterial properties against S. aureus and P. aeruginosa. This study shows that the improved antibacterial behavior of

GO-coated SS316L can be attributed to the electron transfer from the bacterial membrane to the substrate. The obtained GO-nano films on SS316L substrates were thoroughly characterized in terms of their physicochemical properties (e.g. chemical composition, topography, wettability, electronic properties) and biological performance (interactions with MG63 and bacteria). It was shown that the GO-coated SS316L are hydrophilic and have a higher work function, which is considered a fundamental parameter describing the ability of surfaces to adsorb eucaryotic cells and stimulate redox processes. This modification, induced by GO immobilization, results in remarkable changes in electron transfer at the interface, leading to a bactericidal effect. This work paves the way for future improvements in the surface properties of implants for various biomedical applications, including further commonly applied metallic materials such as CoCr-and Ti-based alloys.

Author Contributions

Published on 01 December 2023. Downloaded by WESTFALISCHE WILHELMS UNIVERSITAT MUNSTER on 12/5/2023 12:01:42 PM

Conceptualization – K. Schickle, M. Gołda-Cępa Data curation - K. Schickle, M. Gołda-Cępa, Z.V. Parlak, N. Grigorev, G. Desante

Formal Analysis - A. Chlanda, K. Neuhaus, C. Schmidt Funding acquisition - A. Kotarba, J. Gonzalez-Julian Investigation - A. Chlanda, K. Neuhaus, S. Neuss, K. Drożdż, W. Pajerski

Methodology - M. Gołda-Cępa, Brzychczy-Włoch, Olga Mazuryk Project administration- K. Schickle, M. Gołda-Cępa

Resources - A. Kotarba, J. Gonzalez-Julian, Brzychczy-Włoch, A. Chlanda

Supervision - K. Schickle, M. Gołda-Cępa
Validation - K. Schickle, M. Gołda-Cępa
Visualization - K. Schickle, M. Gołda-Cępa, N. Amousa
Writing - original draft - K. Schickle, M. Gołda-Cępa

Writing – review & editing - N. Amousa, S. Neuss, M. Esteves-

Oliveira, A. Kotarba, J. Gonzalez-Julian

Conflicts of interest

There are no conflicts to declare.

Acknowledgements

The authors would like to thank K.Kowiorski from Łukasiewicz Research Network - Institute of Microelectronics and Photonics, Materials for Energy SectorResearch Group, Aleja Lotników 32/46, 02-668 Warsaw, Poland, for the synthesis of GO nanoflakes applied in this study.

K.S acknowledges ERS RWTH Aachen for "Theodore von Kármán Fellowship – visiting scholars' program for outgoing scientists" for financial support (No. GSO072) of her scientific stay at Faculty of Chemistry, Jagiellonian University in Krakow in Prof. Kotarba's research group.

A.K. would like to acknowledge National Science Centre, Poland for financial support under grant no. 2020/37/8/\$75/034\$9545 The BX63 fluorescence microscope (Olympus) used in the research has been funded from the budget of the qLIFE Priority Research Area under the Strategic Program Excellence Initiative at Jagiellonian University.

Notes and references

- H. Hermawan , D. Ramdan, J.R. Djuansjah. Metals for biomedical applications. Biomedical engineering-from theory to applications, 2011, 1, 411-430.
- 2. A. Marquez, M. Mencia, C. Maharaj. Failure Analysis of a Stainless Steel Hip Implant. Journal of Failure Analysis and Prevention, 2023, 23(2), 846-852.
- B. Akhavan, S. Bakhshandeh, H. Najafi-Ashtiani, A.C. Fluit, E. Boel, C. Vogely, ... S.A. Yavari. Direct covalent attachment of silver nanoparticles on radical-rich plasma polymer films for antibacterial applications. Journal of Materials Chemistry B, 2018, 6(37), 5845-5853.
- B. Akhavan, T.D. Michl, C. Giles, K. Ho, L. Martin, O. Sharifahmadian, ... M.M. Bilek. Plasma activated coatings with dual action against fungi and bacteria. Applied Materials Today, 2018, 12, 72-84.
- C. Stewart, B. Akhavan, S.G. Wise, M.M. Bilek. A review of biomimetic surface functionalization for boneintegrating orthopedic implants: Mechanisms, current approaches, and future directions. Progress in Materials Science, 2019 106, 100588.
- A. Jaggessar, H. Shahali, A. Mathew, P.K. Yarlagadda. Bio-mimicking nano and micro-structured surface fabrication for antibacterial properties in medical implants. Journal of nanobiotechnology, 2017, 15, 1-
- N. Tasnim, A. Kumar, B. Joddar. Attenuation of the in vitro neurotoxicity of 316L SS by graphene oxide surface coating. Materials Science and Engineering: C, 2017, 73, 788-797.
- J.M. Kwak, J. Kim, C.S. Lee, I.S. Park, M. Lee, D.H. Min, I.S.L. Yeo. Graphene Oxide as a Biocompatible and Osteoinductive Agent to Promote Implant Osseointegration in a Rabbit Tibia Model. Advanced Materials Interfaces, 2022, 9(28), 2201116.
- S. Rahpeima, E.M. Dief, S. Ciampi, C.L. Raston, N. Darwish. Impermeable Graphene Oxide Protects Silicon from Oxidation. ACS Applied Materials & Interfaces, 2021, 13(32), 38799-38807.
- J.S. Bunch, S.S. Verbridge, J.S. Alden, A.M. Van Der Zande, J.M. Parpia, H.G. Craighead, P.L. McEuen. Impermeable atomic membranes from graphene sheets. Nano letters, 2008, 8(8), 2458-2462.
- Z. Yang, X. Liu, J. Wu, X. Zhu, Z. Bai, Z. Yu. Preparation of β-cyclodextrin/graphene oxide and its adsorption properties for methylene blue. Colloids and Surfaces B: Biointerfaces, 2021, 200, 111605.

Journal Name ARTICLE

- M. Cacaci, C. Martini, C. Guarino, R. Torelli, F. Bugli, M. Sanguinetti. Graphene oxide coatings as tools to prevent microbial biofilm formation on medical device. Advances in Microbiology, Infectious Diseases and Public Health, 2021, 21-35.
- P. Zhang, Z. Guo, C. Chen, I. Lynch. Uncertainties in the antibacterial mechanisms of graphene family materials. Nano Today, 2022, 43, 101436.
- 14. M.S. Khan, H.N. Abdelhamid, H.F. Wu. Near infrared (NIR) laser mediated surface activation of graphene oxide nanoflakes for efficient antibacterial, antifungal and wound healing treatment. Colloids and Surfaces B: Biointerfaces, 2015, 127, 281-291.
- X. Zou, L. Zhang, Z. Wang, Y. Luo. Mechanisms of the antimicrobial activities of graphene materials. Journal of the American Chemical Society, 2016, 138(7), 2064-2077.
- 16. S.C. Smith, D.F. Rodrigues. Carbon-based nanomaterials for removal of chemical and biological contaminants from water: a review of mechanisms and applications. Carbon, 2015, 91, 122-143.
- R. Li, N.D. Mansukhani, L.M. Guiney, Z. Ji, Y. Zhao, C.H. Chang, ... T. Xia. Identification and optimization of carbon radicals on hydrated graphene oxide for ubiquitous antibacterial coatings. ACS nano, 2016, 10(12), 10966-10980.
- P. Zhang, Z. Guo, C. Chen, I. Lynch. Uncertainties in the antibacterial mechanisms of graphene family materials. Nano oday, 2022, 43, 101436.
- M. Golda-Cepa, K. Syrek, M. Brzychczy-Wloch, G.D. Sulka, A. Kotarba. Primary role of electron work function for evaluation of nanostructured titania implant surface against bacterial infection. Materials Science and Engineering: C, 2016, 66, 100-105.
- W. Pajerski, J. Duch, D. Ochonska, M. Golda-Cepa, M. Brzychczy-Wloch, A. Kotarba. Bacterial attachment to oxygen-functionalized graphenic surfaces. Materials Science and Engineering: C, 2020, 113, 110972.
- G. Desante, N. Labude, S. Rütten, R. Kaufmann, R. Zybała, ... K. Schickle. Graphene oxide nanofilm to functionalize bioinert high strength ceramics. Applied Surface Science, 2021, 566, 150670.
- K. Kowiorski, M. Heljak, A. Strojny-Nędza, B. Bucholc, M. Chmielewski, M. Djas, ... A. Chlanda. Compositing graphene oxide with carbon fibers enables improved dynamical thermomechanical behavior of papers produced at a large scale. Carbon, 2023, 206, 26-36.
- 23. C.A. Schneider, W.S. Rasband, K.W. Eliceiri. NIH Image to ImageJ: 25 years of image analysis. Nature methods, 2012, 9(7), 671-675.
- 24. M. Finšgar, J. Jackson. Application of corrosion inhibitors for steels in acidic media for the oil and gas industry: A review. Corrosion science, 2014, 86, 17-41.
- S.M. Bhagat, D.G. Kolhatkar, A.R. Unchadkar, M.N. Deshpande. Study of organic compounds containing NH₂ and COOH groups as corrosion inhibitor. Oriental Journal of Chemistry, 2010, 26(2), 649.

- 26. X. Shen, X. Lin, N. Yousefi, J. Jia, J.K. Kim vi Mrinkling iip graphene sheets and graphene രജിൻ ഉപ്പെട്ടു ഉപ്പെട്ടു 2014, 66, 84-92.
- 27. M.Z. Miskin, C. Sun, I. Cohen, W.R. Dichtel, P.L. McEuen. Measuring and manipulating the adhesion of graphene. Nano letters, 2018, 18(1), 449-454.
- 28. L. Shi, J. Chen, L. Teng, L. Wang, G. Zhu, S. Liu ... L. Ren. The antibacterial applications of graphene and its derivatives. Small, 2016, 12(31), 4165-4184.
- C.N.R. Rao, R: Voggu. Charge-transfer with graphene and nanotubes. Materials today, 2010, 13(9), 34-40;
- 30. Annual Epidemiological Report 2016 Surgical site infections. https://www.ecdc.europa.eu/en/annual-epidemiological-reports (2017).
- 31. M.Z.I. Nizami, S. Takashiba, Y. Nishina. Graphene oxide: A new direction in dentistry. Applied Materials Today, 2020, 19, 100576.
- T. Zhang, P.L. Tremblay. Graphene: an antibacterial agent or a promoter of bacterial proliferation? IScience, 2020, 23(12), 101787.
- A.I. Banasiak, A. Racki, M. Małek, A. Chlanda. Flake graphene as an efficient agent governing cellular fate and antimicrobial properties of fibrous tissue engineering scaffolds—A review. Materials, 2022 15(15), 5306.
- 34. J. Li, G. Wang, H. Zhu, M. Zhang, X. Zheng, Z. Di, ... X. Wang. Antibacterial activity of large-area monolayer graphene film manipulated by charge transfer. Scientific reports, 2014, 4(1), 1-8.
- 35. D.T. Phan, G.S. Chung. P—n junction characteristics of graphene oxide and reduced graphene oxide on n-type Si (111). Journal of Physics and Chemistry of Solids, 2013, 74(11), 1509-1514.
- W. Pajerski, P. Chytrosz-Wrobel, M. Golda-Cepa, M. Pawlyta, W. Reczynski, D. Ochonska, ... A. Kotarba. Opposite effects of gold and silver nanoparticle decoration of graphenic surfaces on bacterial attachment. New Journal of Chemistry, 2022, 46(27), 13286-13295.
- 37. N. Morimoto, T. Kubo, Y. Nishina. Tailoring the oxygen content of graphite and reduced graphene oxide for specific applications. Scientific reports, 2016 6(1), 1-8.
- 38. S. Pei, H.M. Cheng. The reduction of graphene oxide. Carbon, 2012, 50(9), 3210-3228.
- 39. N. Chatterjee, H.J. Eom, J. Choi. A systems toxicology approach to the surface functionality control of graphene–cell interactions. Biomaterials, 2014, 35(4), 1109-1127.